







## A Surface Unfolding Method for Bolus Shaping Using the Mass-spring Model

Rui Li<sup>1</sup> , Qingjin Peng<sup>2</sup> , Harry Ingleby<sup>3</sup> , and David Sasaki<sup>4</sup> 

<sup>1</sup> University of Manitoba, [lir34512@myumanitoba.ca](mailto:lir34512@myumanitoba.ca)

<sup>2</sup> University of Manitoba, [Qingjin.Peng@umanitoba.ca](mailto:Qingjin.Peng@umanitoba.ca)

<sup>3</sup> CancerCare Manitoba, [hingleby@cancercare.mb.ca](mailto:hingleby@cancercare.mb.ca)

<sup>4</sup> CancerCare Manitoba, [dsasaki@cancercare.mb.ca](mailto:dsasaki@cancercare.mb.ca)

Corresponding author: Qingjin Peng, [Qingjin.Peng@umanitoba.ca](mailto:Qingjin.Peng@umanitoba.ca)

**Abstract.** Bolus is commonly used in high-energy radiotherapy to cover the patient surface in treatment. The existing method of bolus shaping is mainly a manual process that is time-consuming and lack of accuracy. A triangular mesh surface unfolding method is introduced in this research for bolus shaping to improve the accuracy. Triangle crossings are applied to reduce the number of iterations in the process of unfolding a complicated mesh surface. A mass-spring model with crossed springs is proposed to optimize initial 2D patches to reduce errors between the initial 3D surface and 2D patches. A disturbing spring is added into the mass-spring model to correct the deformation in the bolus shape and contour to improve the accuracy and efficiency in the optimal search. A hemisphere model and multi-patches nose model are used to verify the proposed methods. Results show that the proposed method is feasible and efficient in bolus shaping.

**Keywords:** Surface unfolding, bolus shaping, mass-spring model.

**DOI:** <https://doi.org/10.14733/cadaps.2020.979-992>

### 1 INTRODUCTION

Bolus is a sheet of material used in high-energy radiotherapy to smooth patients' skin for a desired dose distribution [4, 18]. The bolus should close to the patient underlying tissue without air gaps to achieve a good therapeutic effect [1, 3, 7]. A manual bolus shaping process is mainly used in clinic by cutting commercial material into two-dimensional (2D) shapes of the targeted body area and then wrapping into a three-dimensional (3D) shape to cover the body surface. The bolus produced in this process is inaccurate and time-consuming [8, 15, 16].

There are different methods proposed for the surface unfolding and wrapping process, such as 3D-to-2D and 2D-to-3D processes using in garment industry [5, 6]. In the 3D-to-2D process, 3D garments models are built based on human body data and then unfolded into 2D patches. Clothing materials are cut based on unfolded 2D patches and then sewed into 3D garments in the 2D-to-3D process [23]. The 3D-to-2D and 2D-to-3D processes can be applied in the bolus shaping process.

The human surface can be scanned to generate surface data by a 3D scanner. Unfolded 2D patches are generated by unfolding the 3D surface and then used to form the bolus.

Our previous work applied existing software tools including methods of surface-based unfolding and nodes-based unfolding to unfold 3D surfaces [10]. In addition, a 3D surface was segmented into different numbers of patches to avoid self-overlap and test how many patches can be refolded to form bolus in the high accuracy and less difficulty. Results show that existing software tools can unfold the 3D surface into 2D pieces successfully. But when unfolding the whole 3D surface directly, it may cause self-overlaps. For the segmentation, the more patches allow a higher accuracy, however it is difficult to fold back with too many patches. Thus, the number of patches between 3 and 5 should be used in the process of refolding. The process of bolus shaping is shown in Figure 1.

In the bolus shaping process, the 3D surface unfolding is the most important process that decides accuracy of the bolus. Using the triangular mesh surface, the unfolding process is a vertex to vertex coordinate transformation process from a 3D surface to its corresponding 2D patches. As most surfaces of the human body are non-developable surfaces, they cannot be unfolded without deformation and distortion [25]. A goal for the accuracy of unfolding a non-developable surface is to reduce difference between the original 3D surface and 2D unfolded surface. Several researchers have proposed different methods to reduce this difference.

Wang et al proposed a central triangle method to complete the coordinate transformation process by selecting and unfolding a central triangle first and then unfolding neighbor triangles of the central triangle layer by layer. They applied a mass-spring model to optimize the unfolded 2D patches to increase unfolding accuracy [19]. Li et al improved the coordinate transformation process using triangle strips to unfold the surface strips by strips, which reduced the number of iterations in the surface unfolding process. In addition, they improved the mass-spring model by adding a crossed spring that can not only resist the in-plane tension or compression but also prevent the flattened mesh from stretching [9]. To reduce complexity of the traditional mass-spring model, Liu et al proposed a simplified energy mass-spring model using an innovative energy relaxation process based on the variable step size to improve efficiency [11]. Liu et al built a flattening system for unfolding the sheet metal, they used a central triangle method to unfold the surface layer by layer [12]. A mass-spring model was used with a crossed spring to optimize the unfolded model.

The length control of a common boundary between 2D patches is important in the unfolding process because if difference of the common boundary between 2D patches is too large, it is difficult to wrap the two patches together. Several methods were used to control the length of common boundary. Wang proposed a method of the length-preserved feature curve optimization called WireWarping to control the boundary deformation in a surface unfolding process. They fixed the feature curve in the 3D model to find the corresponding feature curve in 2D patches that have the same length with the feature curve in the 3D model. The 3D model was then unfolded based on the feature curve to make the 2D patches have a common boundary in the same length [20]. Zhang et al improved the WireWarping using a method called WireWarping++ by increasing flexibility in the length control to avoid large distortions of 2D patterns caused by the strict length control. They used a loose control condition to build a corresponding feature curve in 2D patches that can generate a similar length in common boundaries to get 2D patches with the high accuracy after optimization [24]. Zhang et al proposed a multilevel mesh process to improve surface unfolding efficiency using WireWarping to reduce the distortion in product design [22].

Although the existing surface unfolding methods are widely used in different fields such as garment manufacturing [13, 14, 17] and sheet metal shaping processes [2, 12], those methods have following weaknesses. The number of iterations in the coordinate transformation process is very large, which takes much time in the solution search. In addition, when using the mass-spring model to optimize unfolded patches, the efficiency is based on the original unfolded patches. If the original unfolded patches have the large deformation in shapes and contours, it is difficult to obtain an optimal result because virtual forces of the mass-spring model in the boundary are unbalanced.

The mass-spring model always tries to reduce errors by moving positions of inner vertexes. However, shapes and contours of 2D patches have significant impacts on the accuracy when they are folded back to a 3D shape.

To solve the problems, a surface unfolding process is proposed based on the mass-spring model to unfold human surfaces for bolus shaping. To improve the unfolding efficiency from 3D surfaces to 2D patches, triangle crossings are used to reduce the number of iterations. A mass-spring model with crossed springs is introduced for the optimization of 2D patches to reduce the deformation and distortion of unfolded surfaces. To improve the efficiency of contours optimization in 2D patches, a disturbing spring is added into the mass-spring model with crossed springs to change the shape of 2D patches. Detail processes such as the central triangle selection, coordinate transformation order and overlapping correction are also introduced in the unfolding process. Using the proposed method, a bolus shaping process is developed for improving bolus shaping efficiency and accuracy.

Following sections of this paper are organized as follows. Section 2 introduces the proposed method of 3D surface unfolding processes. Section 3 shows the unfolding process of bolus shaping in detail. Section 4 discusses the optimization process to search unfolded patches. Examples are provided to test and verify the proposed method in Sections 5, followed by the summary and further work discussed in Section 6.

## 2 PROPOSED METHODS

The proposed process of unfolding a 3D surface into 2D patches is first to fix a triangle of the 3D surface on a 2D flat datum and then transfer other nodes of the 3D surface onto the 2D datum with less deformation. The transferring process starts at neighboring nodes of the fixed triangle working on a layer by layer process until all nodes are located in the 2D datum. To reduce deformation from the 3D surface to 2D patches, an energy model is applied to adjust the position of nodes in the 2D datum. Triangle strips proposed in [9] can improve efficiency of the surface unfolding process. However, if the number of vertexes in a surface is large, its unfolding efficiency will be affected. To improve the unfolding efficiency, a triangle crossing is proposed to reduce the number of iterations in the coordinate transformation process. A crossed spring based mass-spring model is applied to optimize initial 2D patches to reduce deformation and distortion between the 3D surface and unfolded 2D patches. To increase efficiency of the optimal search, a disturbing spring is added in the mass-spring model to correct deformation in the shape and contour. The proposed unfolding process is illustrated in Figure 2. It contains searching and unfolding the central triangle, central triangle crossing and adjacent triangle crossings hierarchically, and relaxing energy for all unfolded triangles by a mass-spring model with the crossed spring.

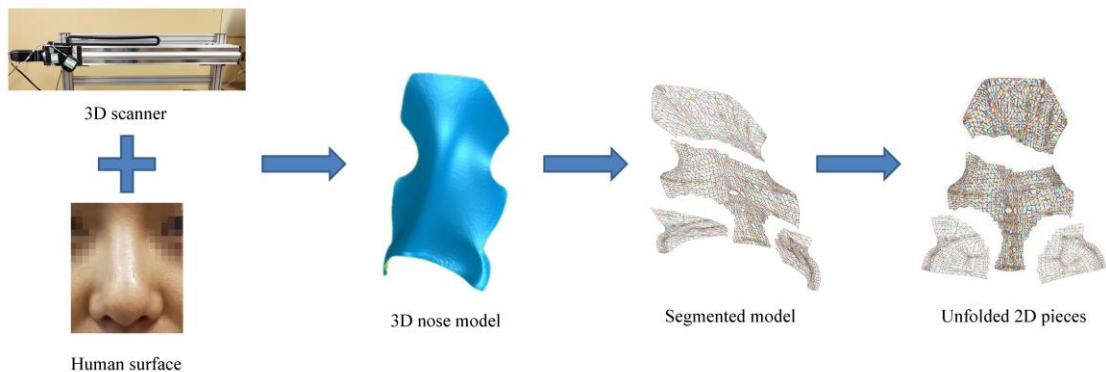


**Figure 1:** Process of bolus shaping.

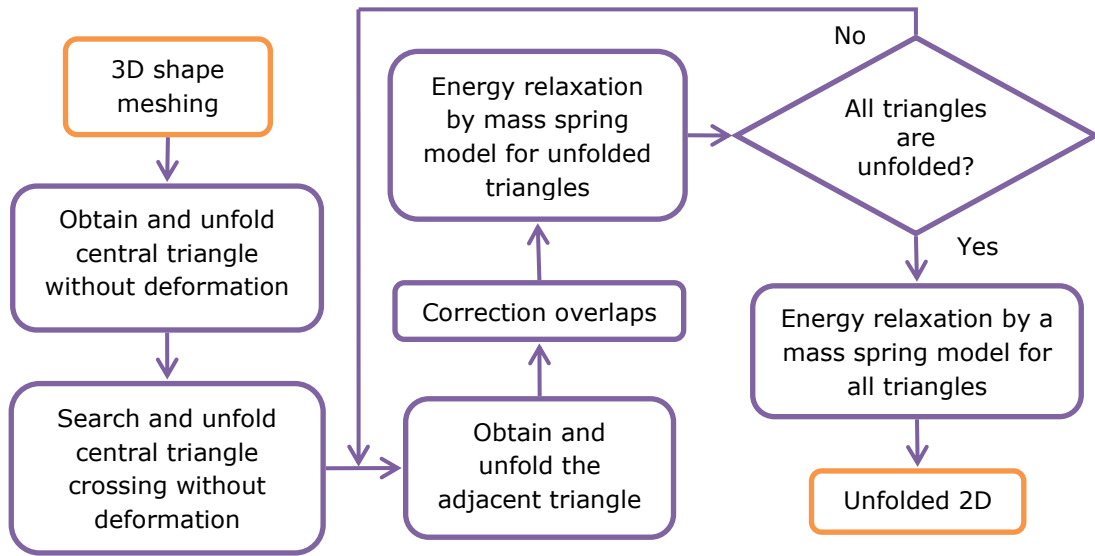


**Figure 2:** Flow chart of the proposed method.

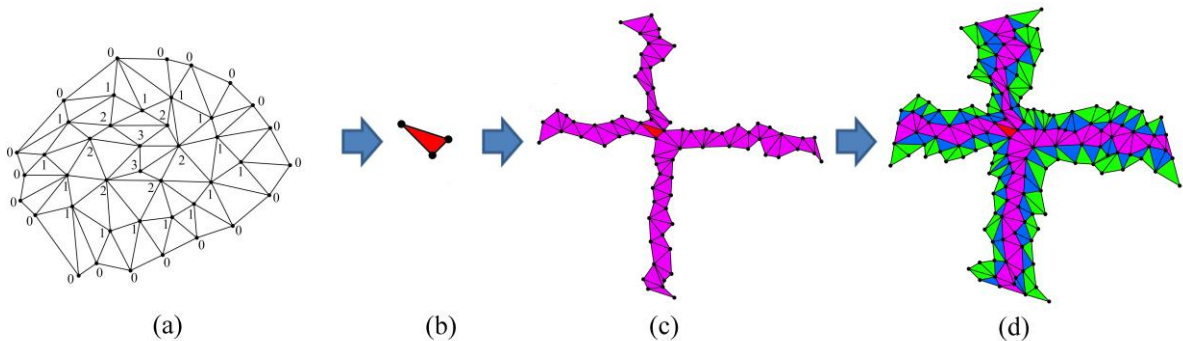


**Figure 3:** Triangle labeling and schematic diagram of triangle crossings. (a) Triangle labeling, (b) Central triangle, (c) Central triangle crossing, (d) General triangle crossings.

### 3 UNFOLDING PROCESS

#### 3.1 Central Triangle Labeling and Unfolding

In the unfolding process, the first step is to select a central triangle and unfold it without deformation. Labels of boundary vertexes are defined as 0, and labels of other vertexes are defined as Inf at first. Vertexes with label Inf that directly connect to boundary vertexes are searched and changed their labels from Inf to 1. Vertexes with label 1 which directly connect to the vertexes with label 1 are searched and changed their labels to 2. Finally, there are no vertexes with label Inf. Labels of each triangle are defined as the summation of labels for vertexes composing of the triangle. The triangle with the largest total label value is chosen as a central triangle. The central triangle is unfolded into a 2D surface without deformation. Figure 3(a) shows the triangle labeling process.

### 3.2 Central Triangle Crossing Selection and Unfolding

To reduce the number of iterations in the coordinate transformation process, a triangle crossing is proposed to increase the number of triangles unfolded in each unfolding step. Figure 3(b)-(d) shows the sequence of triangle crossings, where the pink crossing is the central triangle crossing and other triangles are adjacent triangle crossings.

Thus, after unfolding the central triangle, a central triangle crossing is chosen and unfolded without deformation. The weight center of the central triangle is calculated and several unfolding directions are defined through the weight center of the central triangle. This process starts at the unfolded central triangle, and then searches that whether each edge of unfolded triangle intersects with each unfolding direction. If an edge of an unfolded triangle intersects with the unfolding direction, the neighbor face of the edge will be unfolded. After unfolding triangles pass through each unfolding direction, the total number of triangles in each unfolding direction is calculated. The unfolding direction with most triangles is chosen as a main stripe. The main stripe and its vertical direction are composed as the central triangle crossing. The central triangle crossing is unfolded with no deformation.

If two or more triangles appear as the same value of the label, all the triangles will be unfolded without deformation. All the triangles will be tested to find central triangle crossing. The triangle with the most triangles in the main stripe will be selected as a central triangle.

### 3.3 General Triangle Crossings and Unfolding

To unfold adjacent triangle crossings layer by layer, targeted triangles that will be unfolded in one iterative process should be obtained first. The targeted triangles are 3D triangles having common vertexes with unfolded triangles. Before unfolding targeted triangles, inner angles of targeted triangles should be calculated first. To unfold 3D surface without deformation, the inner angle of a 2D patch should be equal to the corresponding inner angle of the 3D triangle mesh. However, the summed inner angle of an internal vertex in the 3D model may not equal to  $2\pi$  (Equation (1) and Figure 4(a)), while the summed inner angle of an internal vertex in the 2D unfolded surface should equals to  $2\pi$  (Equation (2) and Figure 4(b)). Thus, the method of calculating an inner angle of an internal vertex is shown as follows.

$$\alpha_1 + \alpha_2 + \alpha_3 + \alpha_4 + \alpha_5 + \alpha_6 \neq 2\pi \quad (1)$$

$$\beta_1 + \beta_2 + \beta_3 + \beta_4 + \beta_5 + \beta_6 = 2\pi \quad (2)$$

If  $\beta_1, \beta_2, \beta_3$  have been unfolded,  $\beta_4, \beta_5, \beta_6$  can be calculated as follows.

$$\beta_i = \frac{\alpha_i}{\alpha_4 + \alpha_5 + \alpha_6} \cdot [2\pi - (\beta_1 + \beta_2 + \beta_3)] \quad (3)$$

Where,  $i=4, 5, 6$ .

There are two kinds of targeted triangles in the adjacent triangle crossings. One is triangles with one unfolded edge that belongs to boundaries of unfolded triangles (The blue triangles in Figure 3(d)). The other is triangles only with one unfolded vertex that belongs to boundaries of unfolded triangles (The green triangles in Figure 3(d)).

To calculate the position of unfolded vertexes in targeted triangles, for triangles with one unfolded edge that belongs to boundaries of unfolded triangles, the targeted triangles are blue colored triangles in Figure 5(a), where  $P$  is the vertex to be unfolded,  $\beta_1, \beta_2$  is calculated using Equation (3).  $l_1$  is the length of an unfolded edge of 2D patches. Knowing two angles and one edge of a triangle can uniquely determine a shape of the triangle. After unfolding, vertex  $P$  has two possible positions as shown in Figure 5(a),  $P$  and  $P'$ . To uniquely determine the position of vertex  $P$ , the triangle with the center far away from the center of its adjacent unfolded triangle through the unfolded edge (the orange colored triangle in Figure 5(a)) is chosen as the right triangle position. In Figure 5(a),  $P$  is in the right position.

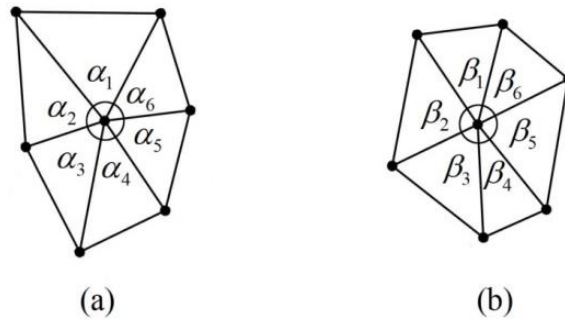


**Figure 4:** Inner angle of 3D model and 2D patches. (a) Inner angle of 3D model, (b) Inner angle of 2D patches.

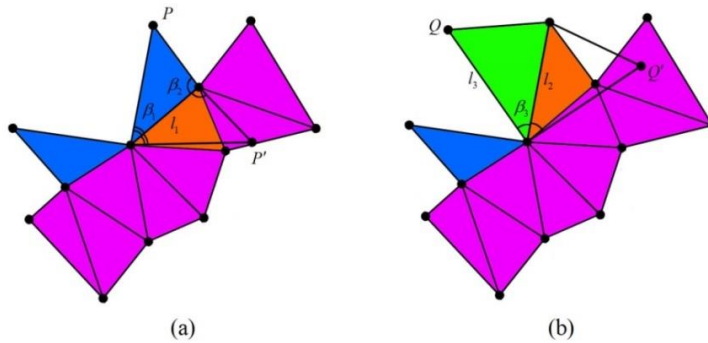


**Figure 5:** Two categories of adjacent triangles. (a) Triangles with one unfolded edge that belongs to boundaries of unfolded triangles, (b) Triangles have only one unfolded vertex that belongs to boundaries of unfolded triangles.

## 4 OPTIMIZATION PROCESS

### 4.1 Mass-spring Model with Crossed Springs

The mass-spring model with crossed springs is applied to control the shape of triangular meshes [9]. The crossed spring-based mass-spring model has the high efficiency in optimizing 2D patches compared to the traditional mass-spring model because the mass-spring model with crossed springs consists of not only virtual masses and tension springs, but also crossed springs. Figure 6 shows the structure of a crossed spring-based mass-spring model. A tension spring connects to two masses along with an edge, which can correct the length deformation of the edge. In addition, a crossed spring connects to two masses by crossing an edge where the two masses are on the edge's neighboring triangles [9].

The topology of a 3D triangular surface is a set  $G = \{V, E, F\}$ , with vertices  $V = \{v_i | v_i \in R^3, 1 \leq i \leq m\}$ , where  $m$  denotes the number of vertices, edges  $E = \{e_{ij} = (v_i, v_j) | v_i, v_j \in V, i \neq j\}$ , and faces  $F = \{f_{ijk} = (v_i, v_j, v_k) | v_i, v_j, v_k \in V, i \neq j, j \neq k, i \neq k\}$ . Relations of vertices, edges, and faces that include vertices of composing edges, vertices of composing faces, edges of composing faces, areas of

faces, length of edges, edges of composing boundary and degrees for each inner angle are built to prepare for unfolding the 3D surface. A pair  $(K, P)$  is used to determine the topological type of a triangular mesh surface  $P = \{P_1, P_2, \dots, P_m\}, P \in R^3$ . The unfolded triangular mesh  $\Phi$  is a pair  $(K, Q)$ ,  $Q = \{Q_1, Q_2, \dots, Q_m\}, Q \in R^2$ . Where,  $K$  expresses the connection of vertices.

Node  $v_0$  is linked to its adjacent node  $v_i$  by edge  $(v_0, v_i)$ . The movement of node  $v_0$  is restricted by the spring force  $f(Q_0, Q_i)$  from springs. For each node  $v_i$ , the total spring force  $\bar{f}(Q_i)$  is calculated as follows.

$$\bar{f}(Q_i) = \sum_{j=1}^N c(|Q_i Q_j| - D_{P_i P_j}) \bar{n}_{Q_i Q_j} \tag{4}$$

Where  $c$  is the stiffness coefficient;  $|Q_i Q_j|$  is the length between unfolded nodes  $Q_i$  and  $Q_j$  in 2D patches;  $D_{P_i P_j}$  is the distance between original nodes  $P_i$  and  $P_j$  in a 3D surface;  $\bar{n}_{Q_i Q_j}$  is the force direction;  $N$  is the number of one-ring neighboring nodes for  $Q_i$ .

The Lagrange equation is used to release energy in the mass-spring model as follows.

$$M\ddot{x} + Kx = 0 \tag{5}$$

Where  $M$  is mass,  $Kx$  is equal to  $-\bar{f}$ .

Euler's method is used to solve Equation (5). It is assumed that the acceleration of mass  $Q_i$  is constant when  $\Delta t$  is very small. For each node  $Q_i$ , mass  $m_i$  can be written as Equation (6).

$$m_i = \frac{1}{3} \rho \sum A_k \tag{6}$$

Where  $\rho$  is the area density.  $A_k$  is the area of one-ring neighboring triangle of node  $Q_i$ .

According to Newton's law, acceleration  $\ddot{x}_i$  at node  $Q_i$  can be calculated by Equation (7).

$$\ddot{x}_i(t) = \frac{f_i(t)}{m_i} \tag{7}$$

Position  $x_i(t_{n+1})$  and velocity  $\dot{x}_i(t_{n+1})$  at step  $n+1$  can be calculated based on position  $x_i(t_n)$ , velocity  $\dot{x}_i(t_n)$ , and acceleration  $\ddot{x}_i(t_n)$  at a time step  $n$  as shown in Equations (8) and (9). The new spring force is updated using Equation (4) based on results in Equation (9).

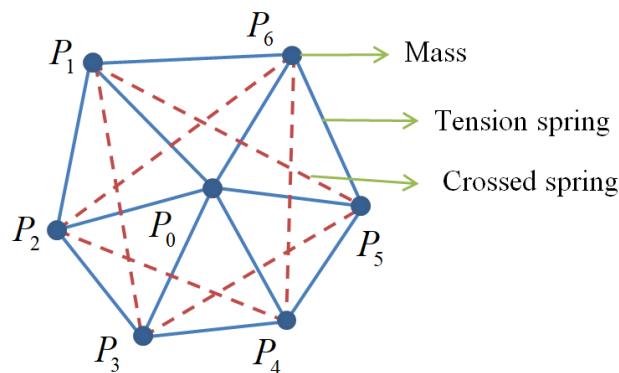


**Figure 6:** Mass-spring model with crossed springs.



$$\dot{x}_i(t_{n+1}) = \dot{x}_i(t_n) + \Delta t \cdot \ddot{x}_i(t_n) \quad (8)$$

$$x_i(t_{n+1}) = x_i(t_n) + \Delta t \cdot \dot{x}_i(t_n) + \frac{1}{2} \Delta t^2 \cdot \ddot{x}_i(t_n) \quad (9)$$

Deformations of edge lengths are shown by the elastic deformation energy  $E(Q_0, Q_i)$ . The total elastic energy  $E(Q_i)$  is calculated by Equation (10).

$$E(Q_i) = \sum_{j=1}^N \frac{1}{2} c (|Q_i Q_j| - D_{p,p_j})^2 \quad (10)$$

The objective of optimization is to minimize the total energy of the whole triangular mesh surface. The total energy  $E_{\text{total}}$  is calculated by Equation (11).

$$E_{\text{total}} = \sum_{i=1}^m E(Q_i) \quad (11)$$

Where,  $m$  is the total number of nodes in the whole mesh surface.

## 4.2 Disturbing Spring

In Figure 7,  $v_1$  is a boundary node and  $v_2$  is an inner node. It shows that the virtual force of the mass-spring model with a crossed spring in the boundary node is unbalanced compared to inner nodes. Thus, the mass-spring model always tries to reduce errors by moving the positions of inner vertexes. Shapes and contours of 2D patches have a significant impact on the accuracy of their folding back to the 3D shape. Thus, if the original unfolded patches have large deformation in shapes and contours, it is difficult to get an optimal result. A disturbing spring is added in some important parts of 2D patches such as the length, width and contour to improve optimization results.

In Figure 7, the red line shows the disturbing spring for controlling shape and blue line shows the disturbing spring for controlling contours. Two boundary vertexes  $v_{b1}$  and  $v_{b2}$  are linked by a disturbing spring. If  $v_{b1}$  is fixed, the movement of node  $v_{b2}$  is restricted by the spring force  $f(v_{b1}, v_{b2})$  from springs and calculated by Equation (12).

$$\vec{f}(v_{b2}) = c \left( \sum |v_{b1} v_{bj}| - \sum D_{bibj} \right) \vec{n}_{v_{b1} v_{b2}} \quad (12)$$

Where  $c$  is the stiffness coefficient;  $\sum |v_{b1} v_{bj}|$  is the sum length between unfolded nodes  $v_{b1}$  and  $v_{b2}$  in 2D patches;  $\sum D_{bibj}$  is the sum distance between original nodes  $v_{b1}$  and  $v_{b2}$  in a 3D surface;  $\vec{n}_{v_{b1} v_{b2}}$  is the force direction. Newton's law is used to calculate the new position of node  $v_{b2}$  using the same process in Section 4.1. With the disturbing spring, the deformation in 2D patches can be reduced, and efficiency of the optimization process can be improved.

## 4.3 Accuracy Measurement

To evaluate the accuracy of unfolded 2D patches, two types of errors are proposed including the length error EL and area error EA as follows.

$$EL = \frac{\sum |L - L_0|}{\sum L_0} \quad (13)$$

$$EA = \frac{\sum |A - A_0|}{\sum A_0} \quad (14)$$

Where  $L_0$  and  $A_0$  are the edge length and triangle area on the triangular mesh 3D surface.  $L$  and  $A$  are the corresponding edge length and triangle area in unfolded 2D patches.



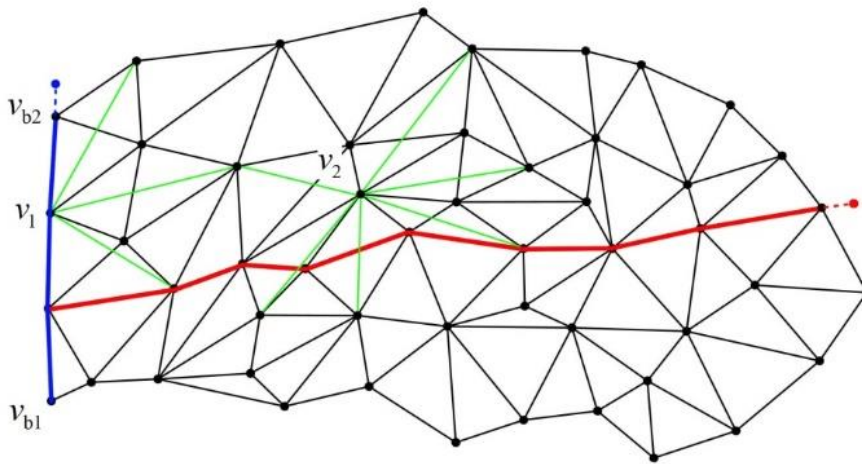


**Figure 7:** Disturbing spring.

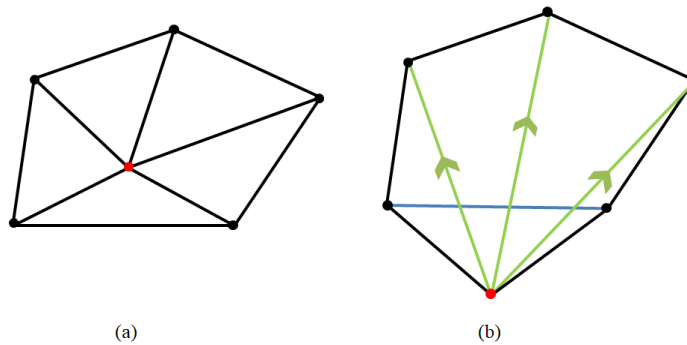


**Figure 8:** Unfolded 2D patches. (a) Unfolded 2D patches without overlaps, (b) Unfolded 2D patches with overlaps.

#### 4.4 Overlapping Correction

In the unfolding process, overlaps of 2D patches may be generated as the accumulation of deformations when more triangles are unfolded. Two methods are used to avoid overlapping. First one is a local algorithm for searching and optimizing overlaps. Second applies the energy release by mass-spring model to reduce deformation of each triangle crossing in the unfolding process.

The first method uses a local algorithm to optimize the unfolding process to avoid overlaps. Figure 8 shows examples of unfolded 2D patches without and with overlaps.

With the occurrence of overlaps, wrong positioned vertexes have two features. First is that the one-ring-neighbor edges of a wrong positioned node have a large error in the length accuracy, and the one-ring-neighbor faces of a wrong positioned node have a large error in the area accuracy. Second is that the one-ring-neighbor edges of a wrong positioned node intersect with other edges (Blue edges in Figure 8(b)). Thus, nodes with overlaps are searched based on those two features.

To correct the wrong positioned node to the right position, one-ring-neighbor edges of a wrong positioned node intersected with other edges (green edges in Figure 8(b)) are selected and assumed as the springs. The direction of the spring force is along edges with the direction of

moving wrong positioned vertexes closed to edges (the arrow direction in Figure 8(b)). After iterating several times, the vertex in the wrong position will be corrected to the right position.

The second method to prevent overlaps using the mass-spring model shown in Section 4.1 to optimize unfolded triangles after unfolding each adjacent triangle crossing to reduce deformation in the unfolding process, which can reduce the accumulation of deformations and decrease the possibility of occurring overlaps.

## 5 CASE STUDY

The surface unfolding process has been coded in Matlab 2017. Two cases including a hemisphere model and a multi-patches nose model are unfolded using the proposed process. In this research, the fallentability proposed in [21] is applied to indicate the developable ability. Figures 9(a) and (b) show that if the summary inner angle of a surface equals to  $2\pi$ , the surface can be unfolded without deformation. The fallentability at a vertex is defined as  $\varpi(v) = |\theta(v) - 2\pi|$ , where  $\theta(v)$  is the summary of inner angles at vertex  $v$ . A smaller surface fallentability means that the surface can be unfolded into 2D patches with less deformation and distortion.

Hemisphere is a typical undevelopable surface with a constant Gaussian curvature. The fallentability is 5.9397. Unfolding results of a hemisphere are shown in Figure 10, where (a) is the 3D mesh surface of the hemisphere; (b) is the 2D unfolded patches without the final energy release by the mass-spring model, and (c) shows the optimized 2D unfolded patches. After the final energy release, the length error EL is decreased from 0.1231 to 0.0955, and the area error EA is decreased from 0.2213 to 0.1544. The energy release therefore can improve the unfolding accuracy significantly.

The nose is an irregular surface of the human body. A nose was scanned using a 3D scanner to obtain its 3D data. The data were then modeled to make a 3D printed model for evaluation of the bolus covering accuracy. The flattenability of nose model is shown in Figure 9(c), where the yellow position has a large value of flattenability. The nose model is segmented into 4 parts to reduce the value of fallentability as shown in Figure 11 (a). The total fallentability of the nose model is 7.9636. The multi-patches after the segmentation include 4 parts with fallentability 1.6460, 2.7243, 1.7255 and 1.6917, respectively. The 4 parts of the nose model are unfolded using the proposed method, respectively. The unfolding results of the nose model with multi-patches are shown in Figure 11 (b). After unfolding, the length errors EL for 4 parts are 0.0093, 0.0227, 0.0073 and 0.0075, respectively. The area errors EA are 0.0194, 0.0479, 0.0164 and 0.0186, respectively.

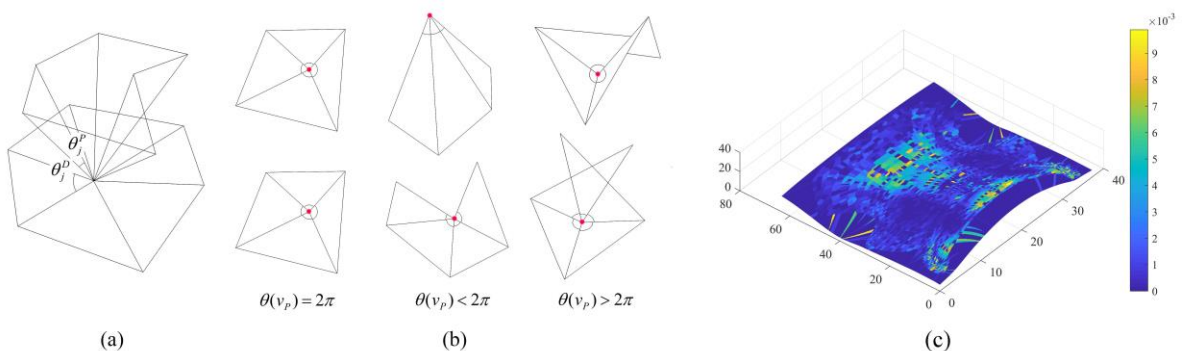


**Figure 9:** Schematic diagram of flattenability and flattenability of nose model. (a) Schematic diagram of unfold triangles, (b) Schematic diagram of different inner angles, (c) Flattenability of nose model.

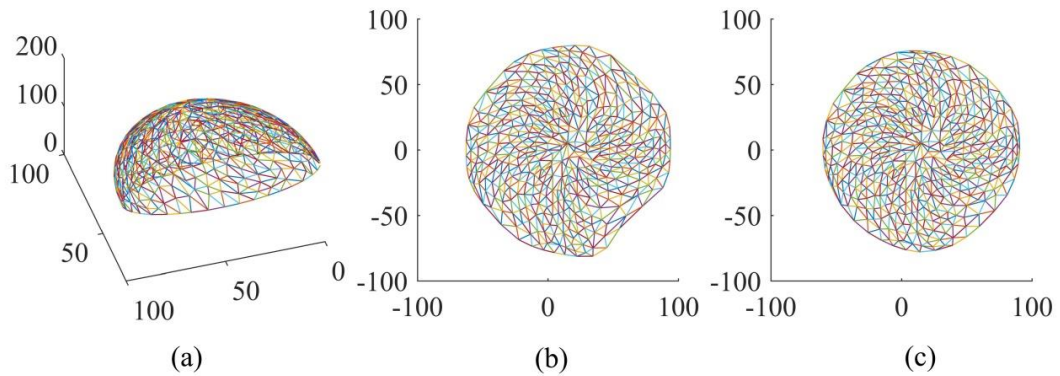


**Figure 10:** A hemisphere model. (a) 3D mesh surface of hemisphere, (b) 2D unfolded patches without final energy release, (c) Optimized 2D unfolded patches.

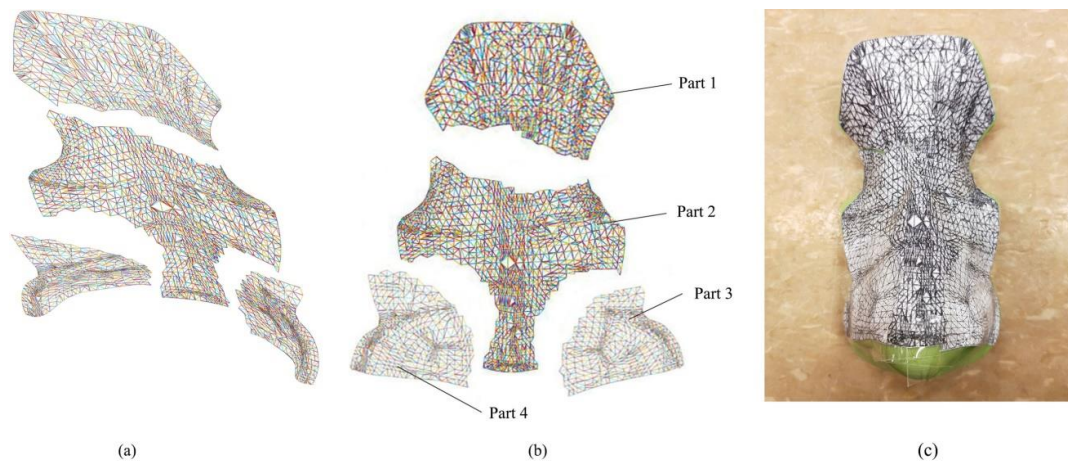


**Figure 11:** A nose model and bolus. (a) 3D models, (b) 2D models, (c) bolus covering on the 3D printed nose model.

To verify efficiency of the proposed triangle crossings method, the number of unfolding layers for triangle strips and triangle crossings are calculated and listed in Table 1. Results show that it needs more layers when using triangle strips to unfold a 3D surface, which may waste much time. Therefore, triangle crossings can reduce the layer of unfolding significantly for the high efficiency.

To further test and verify performance of the proposed unfolding process, a paper-made bolus is formed using the unfolded nose patches. The bolus is covered on the 3D printed nose model to find air gaps between the bolus and nose using a 3D laser scanner. Figure 11 (c) shows the paper bolus covering on the 3D printed nose model.

Scanned surface data of the bolus are aligned with the 3D nose model. Differences are measured using the Control X tool. Figure 12 shows air gaps between two models, where (a) is the 3D deviation; (b) shows the sectional view of symmetry plane of the model, and (c) is the sectional view of plane in the nose bridge. In the 3D deviation, the red color means the largest positive deviation and the blue color means the largest negative deviation. Figure 12(a) shows that the largest positive deviation and largest negative deviation occur near the boundary of nose

surfaces that cannot affect the accuracy of the nose model. The maximum air gap in the nose surface calculated by summing the absolute value of the lower and upper deviations is 2.1501 mm. After the analysis of sectional views of the nose model, the maximum air gap occur in the tip and bridge of the nose.

**6 CONCLUSIONS AND FUTURE WORK**

To obtain accuracy 2D patches for bolus shaping, a 3D surface unfolding method was proposed. Triangle crossings were proposed to improve the efficiency of iterations. A mass-spring model with crossed springs was applied to optimize 2D patches to reduce deformation. To increase the efficiency of optimization, a disturbing spring was added in the mass-spring model to correct the deformation in shapes and contours. Two case examples were tested and verified the proposed method. Results show that the solution meets requirements of bolus shaping. In the further work, the bolus shaping process will be tested in clinic applications using commercial bolus materials. To increase the operability of the proposed bolus shaping process, an automatic design tool of model unfolding and retrieving will be built to be used by medical staff without specific expertise on CAD modelling in bolus forming.

Example	Hemisphere without final energy release	Hemisphere with final energy release	Multi-patches nose model part 1	Multi-patches nose model part 2	Multi-patches nose model part 3	Multi-patches nose model part 4
Fallentability	5.9397		1.6460	2.7243	1.7255	1.6917
Node no.	444		886	1598	811	843
Edge no.	1291		2522	4578	2344	2431
Triangle no.	848		1637	2990	1534	1589
Layer no. of triangle strips	11		8	21	12	11
Layer no. of triangle crossings	7		5	14	8	9
EL (%)	0.1231	0.0955	0.0093	0.0227	0.0073	0.0075
EA (%)	0.2213	0.1544	0.0194	0.0479	0.0164	0.0186

**Table 1:** Length and area errors of the unfolded models.

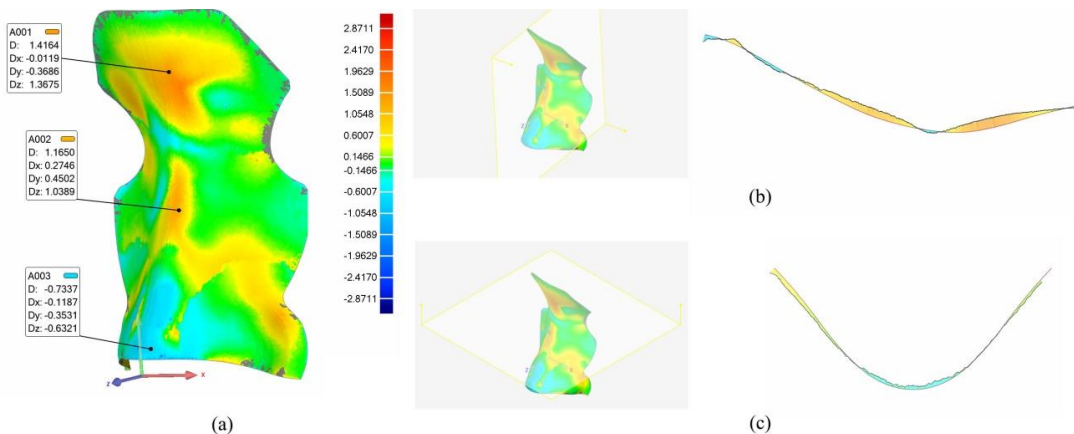


**Figure 12:** Air gaps between the nose model and bolus. (a) 3D deviation, (b) Sectional view of symmetry plane of the model, (c) Sectional view of plane in the nose bridge.

Rui Li, <http://orcid.org/0000-0002-3277-2772>  
 Qingjin Peng, <http://orcid.org/0000-0002-9664-5326>  
 Harry Ingleby, <http://orcid.org/0000-0002-0163-2777>  
 David Sasaki, <http://orcid.org/0000-0002-4233-2543>

## REFERENCES

- [1] Burleson, S.; Baker, J.; Hsia, A. T.; Xu, Z.: Use of 3D printers to create a patient-specific 3D bolus for external beam therapy, *Journal of Applied Clinical Medical Physics*, 16(3), 2015, 166–178. <https://doi.org/10.1120/jacmp.v16i3.5247>
- [2] Cai, Z. Y.; Li, M. Z.; Zhang, H. M.: A simplified algorithm for planar development of 3D surface and its application in the blank design of sheet metal forming, *Finite Elements in Analysis and Design*, 43(4), 2007, 301-310. <https://doi.org/10.1016/j.finel.2006.10.005>
- [3] Canters, R. A.; Lips, I. M.; Wendling, M.; Kusters, M.; van Zeeland, M.; Gerritsen, R. M.; Poortmans, P.; Verhoef, C. G.: Clinical implementation of 3D printing in the construction of patient specific bolus for electron beam radiotherapy for non-melanoma skin cancer, *Radiotherapy and Oncology*, 121(1), 2016, 148–153. <https://doi.org/10.1016/j.radonc.2016.07.011>
- [4] Driscoll, C. F.; Taylor, M. A.; Ostrowski, J. S.: Fabrication of bolus compensators used in the treatment of irregular tissue surfaces in radiation therapy, *Journal of Prosthetic Dentistry*, 67(3), 1992, 370-374. [https://doi.org/10.1016/0022-3913\(92\)90249-A](https://doi.org/10.1016/0022-3913(92)90249-A)
- [5] Hu, S.; Wang, R.; Zhou, F.: An efficient multi-layer garment virtual fitting algorithm based on the geometric method, *International Journal of Clothing Science and Technology*, 29(1), 2017, 25-38. <https://doi.org/10.1108/IJCST-06-2015-0068>
- [6] Huang, H. Q.; Mok, P. Y.; Kwok, Y. L.; Au, J. S.: Block pattern generation: From parameterizing human bodies to fit feature-aligned and flattenable 3D garments, *Computers in Industry*, 63(7), 2012, 680–691. <https://doi.org/10.1016/j.compind.2012.04.001>
- [7] Humphries, S. M.; Boyd, K.; Cornish, P.; Newman, F. D.: Comparison of super stuff and paraffin wax bolus in radiation therapy of irregular surfaces, *Medical Dosimetry*, 21(3), 1996, 155–157. [https://doi.org/10.1016/0958-3947\(96\)00076-3](https://doi.org/10.1016/0958-3947(96)00076-3)
- [8] Kim, S. W.; Shin, H. J.; Kay, C. S.; Son, S. H.: A Customized bolus produced using a 3-dimensional printer for radiotherapy, *PLoS ONE*, (K. Camphausen, ed.), 9(10), 2014, e110746. <https://doi.org/10.1371/journal.pone.0110746>
- [9] Li, J.; Zhang, D.; Lu, G.; Peng, Y.; Wen, X.; Sakaguti, Y.: Flattening triangulated surfaces using a mass-spring model, *The International Journal of Advanced Manufacturing Technology*, 25(1-2), 2005, 108-117. <https://doi.org/10.1007/s00170-003-1818-4>
- [10] Li, R.; Peng, Q.; Ingleby, H.; Sasaki, D.: Methods and analysis of 3D shape unfolding and folding for radiotherapy, In *ASME 2018 International Design Engineering Technical Conferences and Computers and Information in Engineering Conference* (pp. V004T05A023-V004T05A023). American Society of Mechanical Engineers, 2018, 1-10. <https://doi.org/10.1115/DETC2018-85464>
- [11] Liu, Q.; Xi, J.; Wu, Z.: An energy-based surface flattening method for flat pattern development of sheet metal components, *International Journal of Advanced Manufacturing Technology*, 68(5–8), 2013, 1155–1166. <https://doi.org/10.1007/s00170-013-4908-y>
- [12] Liu, X.; Li, S.; Zheng, X.; Lin, M.: Development of a flattening system for sheet metal with free-form surface, *Advances in Mechanical Engineering*, 8(2), 2016, 1687814016630517. <https://doi.org/10.1177/1687814016630517>
- [13] Marconi, M.; Manieri, S.; Germani, M.; Raffaelli, R.: A digitally-enabled integrated approach to design and manufacture shoe lasts, *Computer-Aided Design and Applications*, 16(5-16), 2019, 593-610. <https://doi.org/10.14733/cadaps.2019.593-610>
- [14] Oya, T.; Tanamura, T.; Aoyama, H.; Higashi, M.: Mesh simplification based on feature preservation and distortion avoidance for high-quality subdivision surfaces, *Computer-Aided*



- Design and Applications, 10(3), 2013, 541-550. <https://doi.org/10.3722/cadaps.2013.541-550>
- [15] Park, J. W.; Yea, J. W.: Three-dimensional customized bolus for intensity-modulated radiotherapy in a patient with Kimura's disease involving the auricle, *Cancer/Radiothérapie*, 20(3), 2016, 205-209. <https://doi.org/10.1016/j.canrad.2015.11.003>
- [16] Pugh, R.; Lloyd, K.; Collins, M.; Duxbury, A.: The use of 3D printing within radiation therapy to improve bolus conformity: a literature review, *Journal of Radiotherapy in Practice*, 16(03), 2017, 319–325. <https://doi.org/10.1017/S1460396917000115>
- [17] Thomasse, S.; Bruniaux, P.: A template of ease allowance for garments based on a 3D reverse methodology, *International Journal of Industrial Ergonomics*, 43(5), 2013, 406–416. <https://doi.org/10.1016/j.ergon.2013.08.002>
- [18] Vyas, V.; Palmer, L.; Mudge, R.; Jiang, R.; Fleck, A.; Schaly, B.; Charland, P.: On bolus for megavoltage photon and electron radiation therapy, *Medical Dosimetry*, 38(3), 2013, 268-273. <https://doi.org/10.1016/j.meddos.2013.02.007>
- [19] Wang, C. C. L.; Smith, S. S.-F.; M.F.Yuen, M.: Surface flattening based on energy model, *Computer-Aided Design*, 34, 2002, 823–833. [https://doi.org/10.1016/S0010-4485\(01\)00150-6](https://doi.org/10.1016/S0010-4485(01)00150-6)
- [20] Wang, C. C. L.; WireWarping: A fast surface flattening approach with length-preserved feature curves, *Computer-Aided Design*, 40(3), 2008, 381-395. <https://doi.org/10.1016/j.cad.2007.11.011>
- [21] Wang, C. C. L.: Towards flattenable mesh surfaces. *Computer-Aided Design*, 40(1), 2008, 109–122. <https://doi.org/10.1016/j.cad.2007.06.001>
- [22] Zhang, D.; Li, J.; Wang, J.: Design patterns of soft products using surface flattening, *Journal of Computing and Information Science in Engineering*, 18(2), 2018, 021011. <https://doi.org/10.1115/1.4039476>
- [23] Zhang, M.; Lin, L.; Pan, Z.; Xiang, N.: Topology-independent 3D garment fitting for virtual clothing, *Multimedia Tools and Applications*, 74(9), 2015, 3137-3153. <https://doi.org/10.1007/s11042-013-1774-4>
- [24] Zhang, Y.; Wang, C. C.: Wirewarping++: Robust and flexible surface flattening with length control, *IEEE Transactions on Automation Science and Engineering*, 8(1), 2011, 205-215. <https://doi.org/10.1109/TASE.2010.2051665>
- [25] Zhang, Y.; Wang, C. C.; Ramani, K.: Optimal fitting of strain-controlled flattenable mesh surfaces, *The International Journal of Advanced Manufacturing Technology*, 87(9-12), 2016, 2873-2887. <https://doi.org/10.1007/s00170-016-8669-2>
- [26] Zhao, Y.; Moran, K.; Yewondwossen, M.; Allan, J; Clarke, S.; Rajaraman, M.; Robar, J. L.: Clinical applications of 3-dimensional printing in radiation therapy, *Medical Dosimetry*, 42(2), 2017, 150-155. <https://doi.org/10.1016/j.meddos.2017.03.001>